SAKARYA ÜNİVERSİTESİ
FEN BİLİMLERİ ENSTİTÜSÜ DERGİSİ

Sakarya University Journal of Science
SAUJS

ISSN 1301-4048 e-ISSN 2147-835X Period Bimonthly Founded 1997 Publisher Sakarya University
http://www.saujs.sakarya.edu.tr/

Title: Quantum Efficiency Improvement of InGaN Near Ultraviolet LED Design by Genetic Algorithm

Authors: İrem Ö. ALP, Bilgehan Barış ÖNER, Esra EROĞLU, Yasemin Ö. ÇİFTCİ

Recieved: 2021-12-30 00:00:00

Accepted: 2022-12-05 00:00:00

Article Type: Research Article

Volume: 27
Issue: 1
Month: February
Year: 2023
Pages: 94-112

How to cite
İrem Ö. ALP, Bilgehan Barış ÖNER, Esra EROĞLU, Yasemin Ö. ÇİFTCİ; (2023), Quantum Efficiency Improvement of InGaN Near Ultraviolet LED Design by Genetic Algorithm. Sakarya University Journal of Science, 27(1), 94-112, DOI: 10.16984/saufenbilder.1051252
Access link
https://dergipark.org.tr/en/pub/saufenbilder/issue/75859/1051252

Sakarya University Journal of Science 27(1), 94-112, 2023

Quantum Efficiency Improvement of InGaN Near Ultraviolet LED Design by Genetic Algorithm

İrem Ö. ALP *[1], Bilgehan Barış ÖNER[1], Esra EROĞLU[2], Yasemin Ö. ÇİFTCİ[1]

Abstract

A near-ultraviolet (367-nm) InGaN light-emitting diode (LED) with 5.75 nm quantum well depth was designed and both internal/external quantum efficiency (IQE/EQE) values were optimized considering the effects of non-radiative recombination rates and possible fabrication errors. Firstly, the IQE of the design was enhanced by a genetic algorithm code which was developed particularly for this study. Distributed Bragg Reflectors and optional ultra-thin 1nm AlN interlayer were also used to increase overall light extraction efficiency. Then, alloy and doping concentration effects on wavelength-dependent optical and structural parameters were analyzed via the CASTEP software package based on density functional theory to present a more detailed and realistic optimization. The relatively great values of 42.6% IQE and 90.2% LEE were achieved. The final structure with 1.00 mm × 1.00 mm surface area requires only 200 mW input power to operate at 3.75 V.

Keywords: Light emitting diodes (LEDs), UV-LEDs, near UV devices, solid state devices, GaN-based devices

1. INTRODUCTION

Ultraviolet light-emitting diodes (UV-LEDs) play an important role for a wide variety of usage in semiconductor light technology [1], such as high-resolution data recording, white-light illumination, combined fluorescence/UV-LED systems, and some other application areas in medicine and biochemistry [2-6]. UV-LEDs are also advantageous since being compact, durable, frequency-tunable, low-power required, and eco-friendly on the contrary of conventional bulky toxic gas lasers with low efficiency [7-9].

* Corresponding author: iremoner@gazi.edu.tr (İ Ö ALP)
[1] Gazi University, Faculty of Science, Pyhsics Department, Ankara, Türkiye
E-mail: bbaris.oner@gazi.edu.tr, yasemin@gazi.edu.tr
ORCID: https://orcid.org/0000-0002-6937-7864, https://orcid.org/0000-0001-9440-2235, https://orcid.org/0000-0003-1796-0270
[2] Orta Doğu Teknik Üniversitesi, Mühendislik Fakültesi, Makine Mühendisliği, Ankara, Türkiye
E-mail: esraer@metu.edu.tr
ORCID: https://orcid.org/ 0000-0002-6848-5142

It is known that III-V nitride-based UV-LEDs are promising semiconductor devices among the other UV light sources [10, 11]. Especially, GaN and InGaN with lower indium content are very proper for near UV-LED (NUV-LED) production [12-14]. Because, these materials have a direct band gap and additionally, their emission energy of photons lies between the range of 3.0 - 3.4 eV which corresponds to a region within the near UV limits. This case allows NUV-LEDs with an emission wavelength of 300–400 nm to be used in varying application areas, e.g., identification, illumination, resin curing, and ink-printing [15-18].

GaN-based LEDs are frequently grown on some foreign substrates, such as sapphire, SiC, and Si due to the lack of GaN substrates [19-22]. Even though sapphire is extensively preferred as the substrate for growth of III-group nitrides, a large lattice mismatch issue can occur (over 16% and 13% with GaN and AlN, respectively) [23-25]. This may lead to a high dislocation density, which affects device performance. On the other hand, SiC substrates have a higher lattice mismatch with GaN of ∼3.5% and AlN of ∼1% [1]). Thus, SiC can be a better choice for III-group nitrides compared to sapphire substrates. Even though SiC has many advantages like having almost the same expansion coefficient with AlN and high temperature tolerance, it absorbs the light in the UV region due to the band gap of ∼3.0 eV [26] decreasing the light extraction efficiency (LEE) of UV LEDs. This problem can be solved by distributed Bragg reflectors (DBRs) which exhibit one-dimensional periodicity constituted by materials with lower and higher refractive indices.

DBRs take place between the substrate and main components of LEDs and are utilized for providing a greater amount of reflection of the UV light from the substrate to the device surface whereby the light extraction productivity is enhanced. Because of the above-mentioned features, the III-nitrides DBRs have recently been studied by many researchers [27-29].

A theoretical study on developing high-efficient GaN-based NUV LED considering practical issues has been presented in this paper. Both significant internal and external efficiency improvement were achieved with the help of a genetic algorithm along with an optical analysis. We investigated the light extraction efficiency of InGaN quantum well (QW) placed within p- and n-doped GaN with AlN interlayer (IL) grown on SiC substrate. AlGaN has been used as the electron blocking layer (EBL) due to the extensive direct transition energy range in UV.

In the next section, optimization methods and material analysis of the UV-LED design have been given. Necessary correlations between the different simulation packages were provided. Therefore, a more realistic LED design has been brought out with quite satisfactory results enhanced by DBR, and obtained final structure parameters are given in sub-Section 3.1. Later on, a detailed comparison between the current literature results was given in the Discussion. The device efficiency improvement by possible future innovations was also discussed. Afterward, final remarks were pointed out in the Conclusion.

2. MATERIALS AND METHODS

In this part of the study, we have presented an optimization process beginning from a standard LED design. Mechanical and electronic structure parameters (such as layer widths and doping concentrations) maximizing internal quantum efficiency (IQE) while minimizing the input power requirement were determined and given in the first subsection. In the latter sub-section, revealed material properties were analyzed to obtain corresponding optical properties.

A first optimization step on internal quantum efficiency was employed by the nanostructure quantum electronic simulation

(*nextnano*) [30, 31]. The structural (alloy concentration) and electrical (doping concentration) characteristic effects on optical (refractive index and extinction coefficient) parameters were computed by the CASTEP code [32] based on density functional theory. The related results were transferred to the MPB [33] software for photonic band-gap computations and the MEEP [34] software for electromagnetic wave equation solutions. The details about computation methods have been presented in the related sections.

2.1. Determination of Structural Parameters

A conventional p-i-n LED design consists of an active QW region located between p- and n-doped layers. Electron blocking layers (EBLs) are also usually utilized to increase the performance of the device. Additional semiconductor compounds can also be implemented to reduce non-radiative losses. Even though the whole structure can be complex, essential design parameters can be divided into two main categories in general: mechanical and electronics. In this section, we present an initial optimization process to enhance IQE under these main headlines.

The *nextnano* software program [30, 31] was used for all optoelectronic nano-device simulations addressing IQE improvement. $In_{0.13}Ga_{0.87}N$ was chosen as the material of the QW since we address the NUV region while $Al_{0.66}Ga_{0.34}N$ alloy played the role of the EBL. GaN was chosen as the main III-V semiconductor also for doped layers. The widths of the n-doped and p-doped GaN layers are 3000 and 300 nm, respectively, and kept fixed during the first optimization process. Operating forward potential difference V_{pn} was searched by a scan between 3.0 and 4.0 V for each simulation and only the best of the results minimizing required input power and current densities were taken into account. We have explained the whole process in detail below.

The biggest problem of NUV-LEDs is non-radiative recombination modes. Therefore, we have designed the main structure of the LED to overcome these phenomena from the

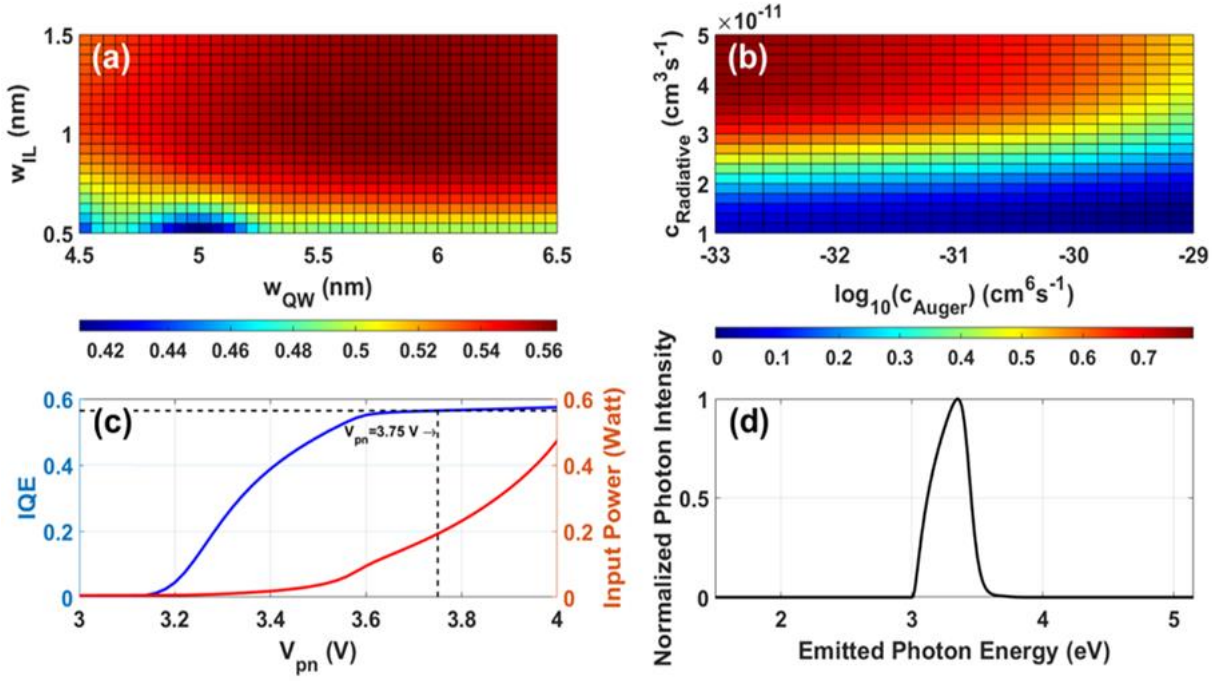

Figure 1 IQE computation results of parameter scanning for (a) quantum well and additional interlayer regions and (b) non-radiative and radiative recombination. (c) The plotted IQE (blue line) and input power (orange line) versus input voltage differences and (d) corresponding emitted photon distribution

beginning. A recent study by Y.-R. Wu et al. [35] demonstrated that choosing relatively thicker QW reduces carrier density in this active region which contributes to prevent non-radiative recombination rates. Another study [36] also showed that an interlayer of III-V compound located adjacent to the QW region has a similar effect. In this manner, the first IQE optimization was performed on the mechanical parameters: the width of the quantum well (W_{QW}), interlayer (W_{IL}), and electron blocking layer (W_{EBL}). Location of the interlayer is decided to be between InGaN quantum well and electron blocking EBL.

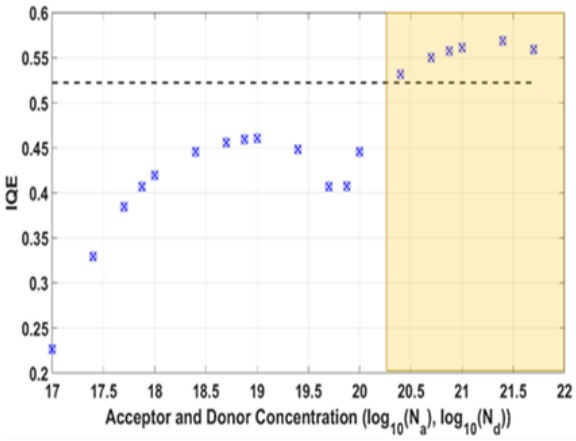

Figure 2 Variation of the internal quantum efficiency versus acceptor/donor (Na/Nd, cm-3) concentration is plotted

The increment of W_{EBL} had a small negative effect on the IQE improvement while significantly decreasing the required input power. This led us to fix the width of this layer at 15 nm and a parameter scan of QW and IL was realized. The results have been shared in Figure 1a and the remaining parameters were chosen the same as of Table 1. The most dominant recombination rates belong to Auger and Shockley–Read–Hall (SRH) recombination modes as mentioned above. Efficiency droop issues of these phenomena are already well-known, however, there are numerous accepted recombination parameters within the NUV region approved by the literature [37-39]. Non-radiative Auger and radiative recombination coefficients were chosen as 1.00×10^{-31} cm^6s^{-1} and 3.00×10^{-11} cm^3s^{-1}, respectively, during the scanning of thickness parameters. Besides, a window of these recombination parameters was scanned and the results for W_{QW}=5.75 nm and W_{IL}=1 nm have been given in Figure 1b. SRH recombination was also considered with default parameters of the related software. Afterward, another optimization was performed on electronic parameters that the width and thickness of the LED were determined as 1.00 mm × 1.00 mm. The operating voltage difference between p-contact and n-contact (V_{pn}) is approximately between 3.10 and 4.22 V, however, IQE saturates after a certain amount of V_{pn} increment. Since power dramatically increases by 56% which corresponds to 97% of the peak value (see Figure 1c). Relatively great internal efficiency was obtained by quite low input power of 200 mW. Also, the corresponding emitted photon distribution was plotted in Figure 1d, and normalized emitted photon energy has a peak at 3.38 eV corresponding to 367 nm approximately.

The parameter scan also gives an idea about possible fabrication errors of thin-film layers of QW and IL regions. According to Figure 1a, the LED structure is quite tolerant of the QW and IL width such that errors up to 35% of both regions still keep the efficiency over 50%. Besides, accurate fabrication of 1 nm AlN interlayer within GaN type hetero-structures is possible by MOCVD [40]. We give a small note on this issue in the Discussion section, since epitaxial growth may do not allow the active layer to have this resolution.

A final analysis of electronic parameters was realized by variant acceptor and donor concentrations (N_a and N_d, respectively) within 10^{17} and 10^{22} cm^{-3} concentration range. Even though IQE does not show a monotone behavior concerning doping concentration, it was possible to maximize the efficiency at a peak value between 1.00×10^{21} and 2.50×10^{21} cm^{-3} (see Figure 2).

Herein, N_a was chosen equal to N_d and structural parameters given in Table 1 were used. The shaded region includes the concentration values which are out of experimental limits. However, these values stay out of practically achievable results (or which cannot be obtained experimentally up to now, please see Section 2.2 and 5. Appendix for details).

Table 1 Structure parameters of the IQE optimization process for near UV-LED operating at 367 nm

Parameter	Value
$\mathbf{W_{p\text{-}GaN}}$	300 nm
$\mathbf{W_{EBL}}$	15.0 nm
$\mathbf{W_{IL}}$	1.00 nm
$\mathbf{W_{QW}}$	5.75 nm
$\mathbf{W_{n\text{-}GaN}}$	3.00 μm
$\mathbf{N_a}$	2.00×10^{20} cm^{-3}
$\mathbf{N_d}$	2.00×10^{20} cm^{-3}
$\mathbf{V_{pn}}$	3.75 V
$\mathbf{c_{Auger}}$	1.00×10^{-31} cm^6s^{-1}
$\mathbf{c_{Radiative}}$	3.00×10^{-11} cm^3s^{-1}
IQE	52.2%
Λ	367 nm (3.38 eV)

Therefore, acceptor and donor concentrations are chosen as 2.00×10^{20} cm^{-3}. The upper and lower limits were determined via experimental values in the literature [41-43] and the concentrations were decreased to the extent of the computation capacity. We share the structural parameters of this initial optimization in Table 1 that correspond to a 52.2% inner quantum efficiency. One should note that this efficiency corresponds to the initial structure and final efficiency will be clear after LEE optimization.

Lattice matching has a critical role in the fabrication process beyond the computational model such that efficiencies are reduced by dislocations [44, 45]. Besides, analyzing the optical properties of materials at the operating wavelength has great importance in the current UV-LED design. Therefore, the external quantum efficiency can be optimized by more realistic parameters. Especially, the refractive index $n(\omega)$ and the extinction coefficient $k(\omega)$ play a crucial role in light extraction computation. For this reason, the next sub-section is dedicated to analyses of the lattice and optical properties.

2.2. Computation of Lattice and Optical Properties

The crystal and band structure calculations were sequentially performed by the CASTEP [32] simulation package to search for information on the lattice match and optical parameters of the UV-LED material components. The exchange-correlation (XC) functional was set as Perdew-Burke-Ernzerhof for solids (PBEsol) which is a revised Generalized Gradient Approximation (GGA) [46] with a good performance in determination of lattice properties for the compounds derived from III, IV, and V groups [47-49]. The convergence tolerance quality for full-geometry optimization was selected as *Fine* during computation runs indicating that the maximum energy change, force, stress, and displacement are 10^{-5} eV/atom, 0.03 eV/Å, 0.05 GPa, and 0.001 Å, respectively and the process ends when the obtained values are less than the tolerance. The ultrasoft pseudopotentials were preferred with 450 eV energy cutoff for the plane-wave basis set. Otherwise, based on the main run with PBEsol, a separate XC functional GGA/PBE was used in non-self-consistent mode while analyzing the electronic and optical characteristics to get realistic data as possible. Herein, the empty bands were taken as two times a total valence electron number of the undoped or host compounds for these wide-gap semiconductors.

Initially, p-type Mg:GaN and n-type Si:GaN were modeled with N_a and N_d values of 1.45×10^{21} cm^{-3} and 1.36×10^{21} cm^{-3}, respectively (we were able to carry out simulations within the computational limits allowed by our system). Afterward, these values were fit by a function scanning various

Table 2 Lattice constants, Monkhorst-Pack k-point grid used in calculations, and energy gap (E_{gap}) values for SiC, AlN, AlGaN, GaN, Mg:GaN, and Si:GaN

Bulk Layers of UV-LED	Lattice Constants a (Å)		b (Å)		c (Å)		k-points	E_{gap} (eV)	
	Present	Exp.	Present	Exp.	Present	Exp.		Present	Exp.
6H-SiC (Substrate)	3.082	3.081[51,52]	---	---	15.115	15.120[51] 15.125[52]	16×16×3	2.13	3.00[55]
AlN (Buffer)	3.126	3.110[53,54] 3.112[55]	---	---	5.001	4.980[53,54] 4.982[55]	16×16×10	4.19	6.12[56]
GaN	3.194	3.189[53] 3.190[54]	---	---	5.205	5.185[53] 5.189[54]	16×16×10	1.96	3.40[57]
$Al_{0.66}Ga_{0.34}N$ (EBL)	9.438	---	---	---	5.080	---	5×5×10	3.19	4.99[58]*
Mg:GaN	9.585	---	15.976	---	5.207	---	5×3×10	1.97	---
Si:GaN	12.772	---	15.966	---	5.209	---	4×3×10	1.90	---

* The data is obtained by the relation in Ref. [58] with a bowing parameter of 0.9 eV at 300 K [59] specifically for $Al_{0.66}Ga_{0.34}N$.

** In order to adjust the Mg and Si concentrations, the GaN unitcell was expanded to 3×5×1 and 3×4×1 supercells, respectively. Likewise, $Al_{0.66}Ga_{0.34}N$ was constructed using the 3×3×1 supercell of GaN.

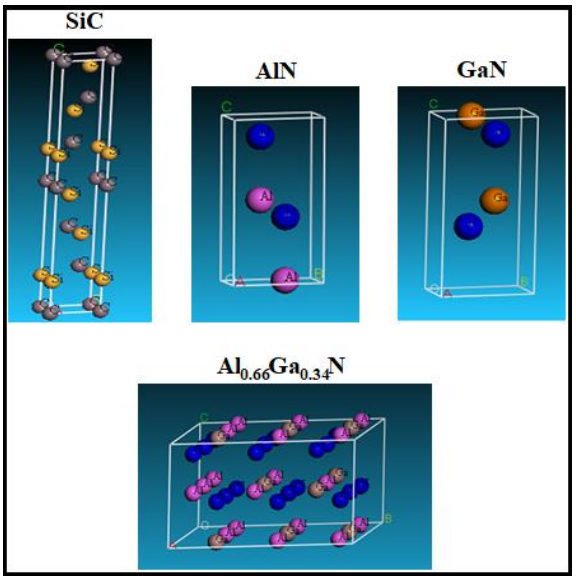

Figure 3 Optimized unit cells of bulk SiC, AlN, GaN and $Al_{0.66}Ga_{0.34}N$ (Yellow: Si, Gray: C, Purple: Al, Brown: Ga and Blue: N)

theoretical and experimental data. Interpolation was performed for the desired concentration value of 2.00×10^{20} cm^{-3} (See Table A1 in *5. Appendix* for details). In the meantime, bulk SiC, AlN, GaN, and $Al_{0.66}Ga_{0.34}N$ were constructed and the optimized unit cells have been given in Figure 3. Moreover, the resulting lattice constants, customized Monkhorst-Pack k-point grid [50], and energy gap (E_{gap}) values have been presented for these bulk layers of UV-LED in Table 2.

The obtained results as seen in Table 2 show that the lattice match is substantially satisfied for the considered material set, which already takes part in various experimental studies [1, 20, 22, 61]. SiC/AlN, SiC/Si:GaN, AlN/$Al_{0.66}Ga_{0.34}N$, and $Al_{0.66}Ga_{0.34}N$/Mg:GaN mismatch percent values are 1.4%, 3.5%, 1.6%, and 0.02%, respectively. The electronic calculation was performed with a different non-local XC functional GGA-PBE [62] expecting to reach much improved optical param- eters [63], but the obtained energy gap values are still less than the literature as seen in Table 2. Then so, the scissors operator (sci-op) [64] within CASTEP was additionally applied in the electronic structure for SiC, AlN, GaN, and $Al_{0.66}Ga_{0.34}N$ to fit the E_{gap} values to the experimental data given at room temperature. It is verified that these compounds can be classified as wide-gap materials as well known; on the other hand, heavily Mg and Si doping of GaN leads to many body interactions and shift of the Fermi energy level of the valence bands up-

ward and conduction bands downward, respectively pointing out degenerate p- and n-type semiconductors [65].

This case prevents utilizing the sci-op for band gap width while this method can be valid for the optical properties. At first, the *n* and *k* parameters measured at 300 K [60] were considered to determine the sci-op value for GaN (sci-op$_{(GaN)}$). It was found to be 0.675 satisfying the best fit with the experimental data. Subsequently, the band gap energies were expanded by sci-op$_{(GaN)}$ / $E_{gap(GaN)}$ to predict sci-op values used in the optical part for Mg:GaN and Si:GaN (N_a=1.45×10^{21} cm^{-3} and N_d=1.36×10^{21} cm^{-3}).

We focused on two significant optical parameters mentioned in the previous section: $n(\omega)$ and $k(\omega)$. The frequency-dependent complex dielectric function $\varepsilon(\omega) = \varepsilon_1(\omega) + i\,\varepsilon_2(\omega)$ referring to the linear response of materials in a weak electromagnetic field was used to compute $n(\omega)$ and $k(\omega)$. In order to have an opinion about optical absorption, the imaginary part $\varepsilon_2(\omega)$ was obtained from the momentum matrix. Coupling the occupied and unoccupied states in valence and conduction bands, respectively, yield in the expression as follows,

$$\varepsilon_2(q \to O_{\hat{u}}, \hbar\omega) = \frac{2e^2\pi}{\Omega\varepsilon_0}\sum_{k,v,c}|\langle\Psi_k^c|\vec{u}\cdot\vec{r}|\Psi_k^v\rangle|^2\,\delta(E_k^c - E_k^v - E) \quad (1)$$

where the incident photon energy is denoted by $\hbar\omega$. e is the electronic charge, Ω is the volume of the reciprocal unit cell (or supercell), and ε_0 is the permittivity of free space. Ψ_k^c and Ψ_k^v are the conduction and valence band wave functions at the k point, $\vec{u}$ and $\vec{r}$ indicate the electric field polarization vector and position operator, respectively. $\delta(E_k^c - E_k^v - E)$ represents for the energy difference between the conduction and valence bands at the k point with the absorption of a photon with energy E. However, the matrix elements of the position operator can be replaced by that of the momentum operator providing calculations in reciprocal space and an additional term of optical matrix elements shows itself in computation results due to the usage of ultrasoft pseudopotentials [66].

$\varepsilon_1(\omega)$ can also be obtained from Eq. 1 through the Kramers-Kronig relation [67] by the following formula:

$$\varepsilon_1(\omega) = 1 + \frac{2}{\pi}P\int_0^\infty \frac{\varepsilon_2(\omega)\omega' d\omega'}{\omega'^2 - \omega^2} \quad (2)$$

where P is the principal value of the integral.

Now, we can write $n(\omega)$ and $k(\omega)$ as a function of frequency as given below:

$$n(\omega) = \left(\frac{\sqrt{\varepsilon_1{}^2(\omega)+\varepsilon_2{}^2(\omega)}+\varepsilon_1(\omega)}{2}\right)^{1/2} \quad (3)$$

$$k(\omega) = \left(\frac{\sqrt{\varepsilon_1{}^2(\omega)+\varepsilon_2{}^2(\omega)}-\varepsilon_1(\omega)}{2}\right)^{1/2} \quad (4)$$

At this point, the quantum well region is not considered due to being considerably small compared to the operating wavelength. In this case, this lay er's effects on reflection and refraction are negligible which can be explained by the effective field theory [68].

Wavelength notation in photonic device literature (such as peak emission) is more common, and so we present the wavelength dependencies of refractive index and extinction coefficient for SiC, AlN, and $Al_{0.66}Ga_{0.34}N$ in Figure 4. The refractive index distribution brings less wavelength dependency and the large distinction of the substrate and buffer indices makes them promising candidates to constitute DBR layers. On this basis, the apparent difference of n values between SiC and AlN creates a great potential for a possible DBR design while high k values of doped regions are not negligible considering the light extraction from the QW layer. Even though materials

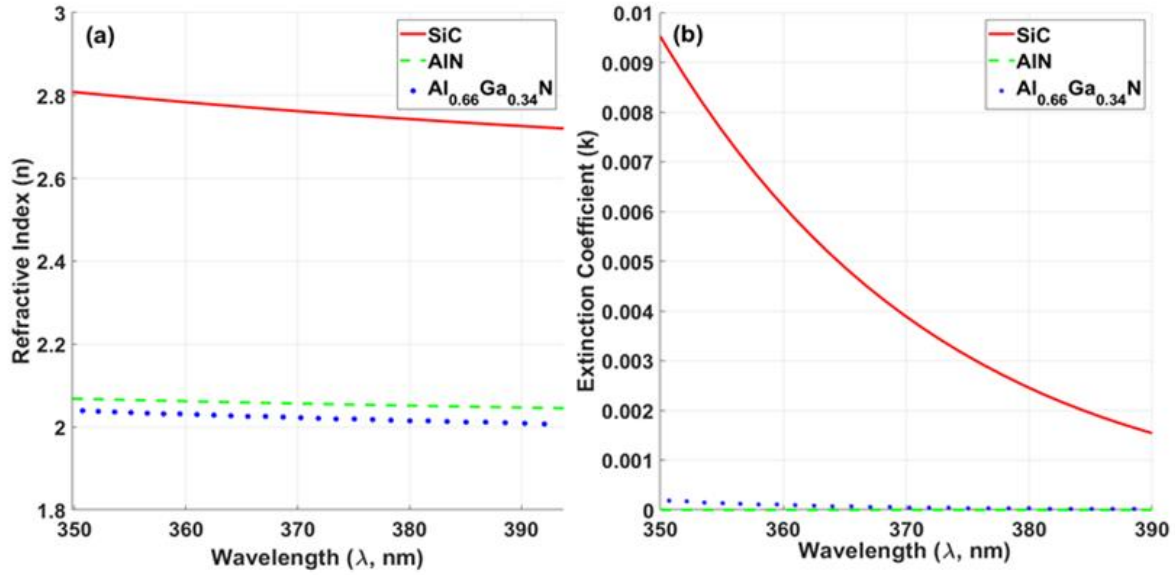

Figure 4 (a) Wavelength dependency of LED layer refractive indices and (b) extinction coefficients

are birefringent by hexagonal crystals, we neglect the radiation through the longitudinal c-axis which does not correspond to the main propagation direction of the emitted light.

Besides, 5. Appendix and Figure 4 also reveal another problem of NUV-LED designs such that the reduced operating wavelength causes a remarkable light absorption by the LED structure itself. A rough estimation of the absorption coefficient, $\alpha=4\pi k/\lambda$, shows that approximately half of the electromagnetic wave diminishes by a 100 nm travel through Mg:GaN.

2.3. Optimization Method

A computational optimization process in this study is unavoidable due to the complex structure of the design solution. Here, the genetic algorithm is distinguished from the other methods due to having the potential of revealing not only local but also global extremum points of random distributions. Efficiency response of acceptor and donor concentrations is only one of the examples of this issue where local extremums do not correspond to the required solution (please see Figure 2).

A differential evolution-based algorithm has the possibility to stick around a local extremum and miss the best result when a multidimensional (structure parameters) computation is performed. On the other hand, fit function of the process can be handled as desired by this algorithm and relatively quick results can be obtained. All of the abovementioned remarks led us to develop an optimization code based on a genetic algorithm to implement on efficiency calculations. The algorithm is based on some main steps given below:

2.3.1. Arbitrarily Generated First Population Headings

An initial population was generated within upper and lower bounds, which come out as physical limitations on the mechanical and optoelectronic parameters. The lower bounds were determined taking fabrication growth resolutions of active region materials [40]. Besides, the upper bounds were given regarding the maximal values available in the literature. Later on, the required codes of *nextnano* software were constructed automatically and performance analysis was carried out.

2.3.2. Computation of Fitness Values

The parameters of each initial structure were assumed as genes of chromosomes (here chromosomes represent a full LED structure). This time, IQE values of the chromosomes were imported from *nextnano* output files to the optimization code and were sorted regarding IQE.

2.3.3. Selection & Crossover

Genetic algorithm gives an extreme opportunity to set algorithm parameters. One of these choices belongs to the selection criteria and further crossover process. In the current study, we have chosen the n^{th} successful chromosome to realize a crossover with $(n\text{-}1)^{th}$. A final crossover was done by the first and the last successful chromosome. This brings another contribution keeping the solution from local extremums and enabling an increment in the average success of each generation. The next generation was constituted by these new chromosomes keeping the population size.

2.3.4. Termination of the Algorithm Headers

The algorithm restarts from the beginning after the previous step and the loop continues until an efficiency criterion is provided. The main limitation on the final success lies beneath the recombination parameters given in Section 2.1. Details of the further improvements in the design had already been mentioned in Section 2.1 and 2.2.

The final structural parameters should be given after light extraction efficiency computation since EQE also depends on LEE. Therefore, we share our final results in Section 3, which utilizes all previous optimization, inner efficiency and material analysis.

3. RESULTS

In the light of the information given in the previous Section, we performed the last part of the optimization to enhance the external quantum efficiency of the design and we present the process with achieved results in the next Section 3.1 with a brief discussion of the literature given in very following subsection.

3.1. Computation and Improvement of External Quantum Efficiency

There are several reasons causing the external efficiency droop. The main loss arises due to the high extinction, and therefore absorption, coefficient values of doped GaN regions. Almost half of the power is lost in a standard design since doped III-V compounds show absorbing feature light in the UV spectrum (see 5. Appendix).

The $W_{n\text{-}GaN}$ and $W_{p\text{-}GaN}$ values should be shortened which causes a partial decrement in IQE. In other words, there is a certain trade-off between IQE and EQE values. We have chosen $W_{n\text{-}GaN}$ and $W_{p\text{-}GaN}$ to be 100 nm and 50 nm, respectively considering this issue. This choice led us to an IQE of 42.6% and light extraction efficiency of 34.6%. Usually, a larger n-layer is chosen in LED designs. This also reduces the dislocation density of the layer at the proximity of the active region. However, in our study we already arrange the lattice matching of Buffer and n-layer materials to minimize dislocations. Moreover, the less electromagnetic wave propagates within the device the better LEE values are obtained. The main reason of this is the nonnegligible extinction coefficients of doped III-V compounds (see 5. Appendix).

Another problem arises on all standard LED designs such that emitted electromagnetic waves from the active region are not guided in general. This causes the light to have arbitrary propagation directions. In this manner, we have proposed one- dimensional photonic crystals, namely DBRs, to be utilized in the design to enhance EQE. It is possible to set the Buffer layer itself as a

multi-layer DBR structure to keep UV-LED compact.

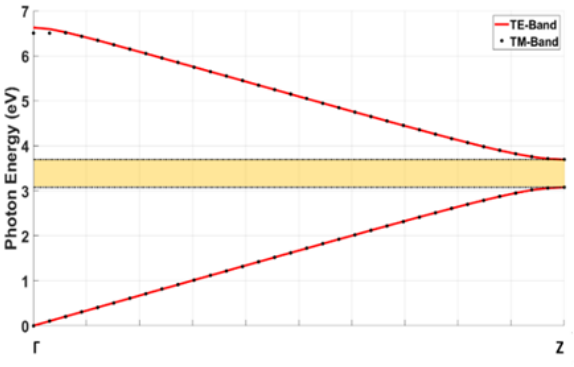

Figure 5 Dispersion diagram of periodic SiC-A1N structure for the light propagation through the periodicity

In Section 2.2, the congruence of SiC and AlN lattice parameters was already mentioned. They also have a remarkable refractive index mismatch which is a crucial need for a standard PC design. Therefore, we have chosen a periodic SiC-AlN sequence as the buffer layer and share the related dispersion diagram in Figure 5. The shaded region represents the photonic bandgap that lies within 3.08 eV (403 nm) - 3.69 eV (336 nm). MPB [33] photonic band-gap software package is utilized in DBR calculations.

One of the advantages of this layer is being almost polarization dependent such that Transverse-Electric and Transverse-Magnetic bands overlap and therefore a common band-gap occurs. The lower and upper bounds of the band-gap region are 336 and 403 nm, respectively while the widths of both AlN and SiC are 38 nm. Figure 6 shows the whole UV-LED structure and external quantum efficiency enhancements by the help of DBR are given in Table 3.

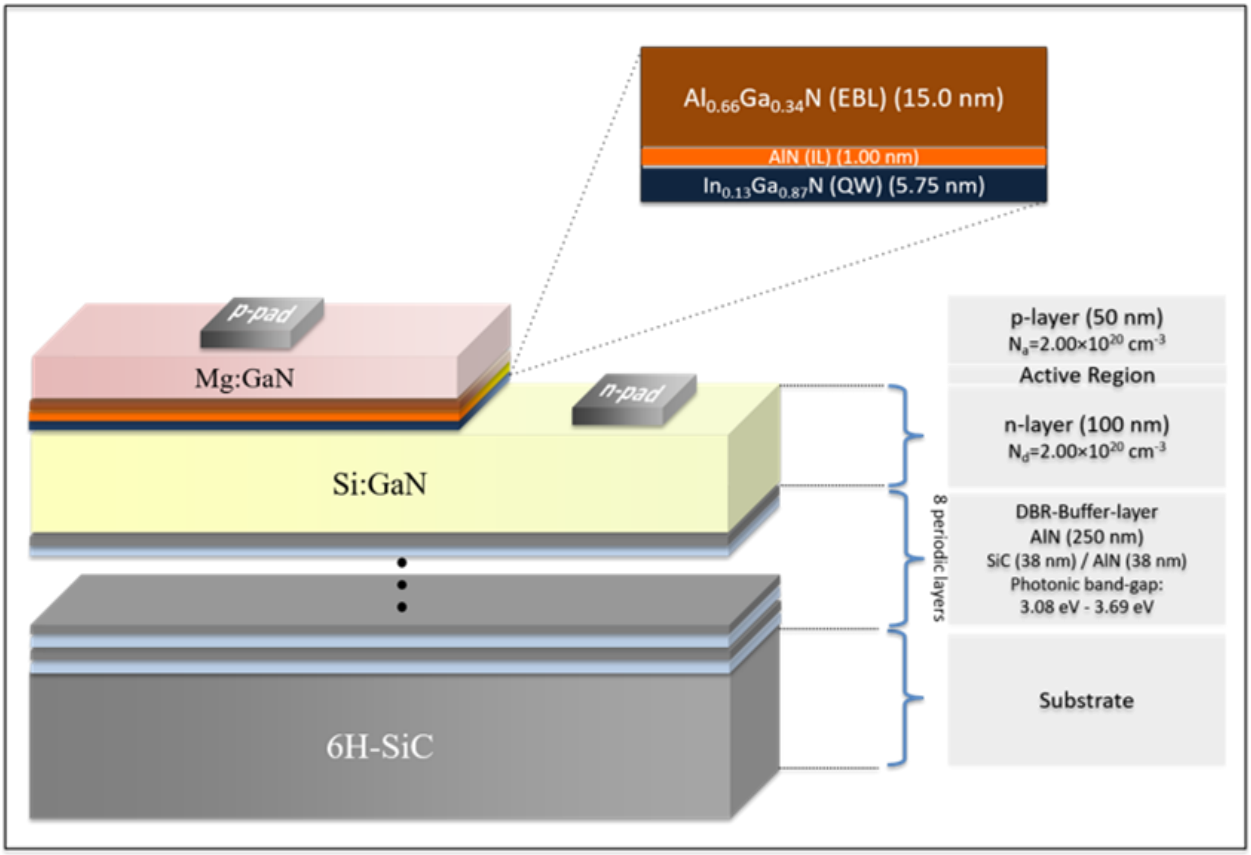

Figure 6 Schematic diagram of the optimized NUV LED design

3.2. Discussion

There have been great attempts to increase internal, external or overall efficiency of LED devices [12, 13, 69-72]. Even though improvement methods can be classified in numerous ways, main concepts include: Alloy composition or layer width modification, non-radiative recombination suppressing and additional / alternative LED layers.

Table 3 The structure parameters of the final optimization process (with DBR) for near UV-LED operating at 367 nm considering both IQE and EQE improvement

Parameter	Value
$W_{p\text{-}GaN}$	50 nm
W_{EBL}	15.0 nm
W_{IL}	1.00 nm
W_{QW}	5.75 nm
$W_{n\text{-}GaN}$	100 nm
N_a	2.00×10^{20} cm^{-3}
N_d	2.00×10^{20} cm^{-3}
V_{pn}	3.75 V
c_{Auger}	1.00×10^{-31} cm^6s^{-1}
$c_{Radiative}$	3.00×10^{-11} cm^3s^{-1}
IQE	42.6%
EQE	38.4%
Wavelength (λ)	367 nm (3.38 eV)

Implementation of additional layers adjacent to the active region has been already a well-known process in the literature [12, 13, 69, 71]. The main reason for this idea lies beneath decreasing non-radiative recombination rates. In this manner, a similar approach was used in a recent study [13], in which an interlayer of gain is utilized to increase LED efficiency. This technique brings a remarkable improvement up to 60%, which is considerably high while the main problem of efficiency droop arises below 370 nm operating wavelength [8]. Even improved performance of InGaN/AlGaN multi quantum well LEDs have an estimated efficiency below 15% [72]. Muramoto et al. [8] set the EQE limit record to 43.2% where the emission wavelength is 375 nm which is quite satisfactory compared to the literature. For example, a recent study revealed the local potential fluctuation effect on radiative recombination increment, which shows a 23.2% IQE and 6.6% LEE [18]. Besides GaN, ZnO-based mechanisms are also good candidates for future UV-application semiconductors [38]. However, low mobility and stronger non-radiative coupling are the apparent shortcomings of these devices [73]. There are also other engineering approaches such as spatial output distribution shaping [70] by nanorods, nevertheless, the UV-LED concept suffers especially from the efficiency droop problem.

The design of the current study was based on the idea of improving the efficiency of a standard single quantum well UV-LED device. In main technique, it was determined to insert additional III-V compound layer within active region and perform parameter optimization. Figure 1 shows that the most distinct advantage of the design is being fabrication-error tolerant. The same figure also reveals that the main limitation on efficiency occurs due to non-radiative effects. Maximizing the efficiency requires heavily doped n- and p-layers while it is still possible to keep IQE over 40% by moderate acceptor and donator levels.

A final note should be given on the ultra-thin interlayer which is optional on standard LED devices. A layer width of 1 nm is realistic only by MOCVD [40] and therefore the design should not include this layer while considering other fabrication methods. Fortunately, the device without AlN interlayer still has a great computational inner efficiency over 40% with operating wavelength around ~370 nm. Since this wavelength is much greater than 1 nm, the AlN interlayer does not have any effect on external efficiency computations.

4. CONCLUSION

This study addresses both internal and external quantum efficiency improvement of

near ultraviolet LED design. This dual analysis method carries extreme importance since some of the parameters like layer widths and concentration rates affect both IQE and EQE values dramatically. Practicality of the UV-LED device reveals additional problems to be handled. In this manner, a computational optimization method should be included because of the relatively complex solution requirement. A genetic algorithm has been developed and implemented to the inner efficiency analyses to overcome this problem and impressive results pushing the theoretical limits were obtained.

The advantage of the design is not limited only by efficiency improvement. Lattice matching between all sequential layers of GaN-based UV-LED minimizes possible losses due to dislocations. Also, fabrication-error tolerance of the device is quite satisfactory. Considering wavelength and alloy/dopant concentration dependent $n(\omega)$ and $k(\omega)$ values besides non-radiative recombination increased the coherence of the results with that of experimental ones. A wavelength window of 350-390 nm was analyzed since this corresponds to a certain part of the NUV region where the emission peak wavelength falls within.

A sole IQE optimization leads the efficiency up to 52%, while including reflection and absorption effects of GaN-based materials puts the structure in its final form with 42.6% IQE and 90.2% LEE. Thus, we conclude that it is possible to enhance the overall efficiency of GaN-based UV LEDs considering both internal and external efficiency improvement with the help of a genetic algorithm supported by a material analysis.

5. APPENDIX

Both the change of refractive index and extinction (also absorption) coefficient of a semiconductor is nonnegligible while N_a or N_d is greater than 10^{16} cm^{-3} and can be quite large for heavily doped materials: N_a or $N_d \gg 10^{18}$ cm^{-3}. *n* and *k* have distributions with respect to the acceptor and donor concentrations such that they have turning points on a critical value N_c. There are only a few researches covering this issue and related distributions within the UV region in the literature for the materials utilized in this study [60, 74-79] and especially Ref. [80] shows its effect on optical parameters clearly.

Experimental data of extinction coefficients in the proximity of operating wavelength were found as 0.190 and 0.112 for Mg:GaN and Si:GaN, respectively [76, 80]. As for refractive index, no certain *n* values (corresponding operating wavelength and concentration) are available in the literature and computation can only be performed up to a certain limit regarding concentration ratio of Mg and Si doped GaN layers (see Section 2.2). Therefore, an analysis, building a bridge between computational and experimental data was set for *n* distributions for a possible curve fit. It was observed that a modified negative Landau distribution was one of the most proper choices as a fitting function:

$$f(x) = c - e^{(a_1(x-\mu)-e^{a_2(x-\mu)})/a_3} \qquad (5)$$

where c and μ correspond to the GaN refractive index and critical concentration value, respectively, whereas $x = log_{10}(N)$. Refractive indices for Mg:GaN and Si:GaN with respect to varying acceptor and donor concentrations were given in Figure A1. Values larger than 2.00×10^{20} cm^{-3} were computed by CASTEP and the other data were taken from experimental values [60, 74-80].

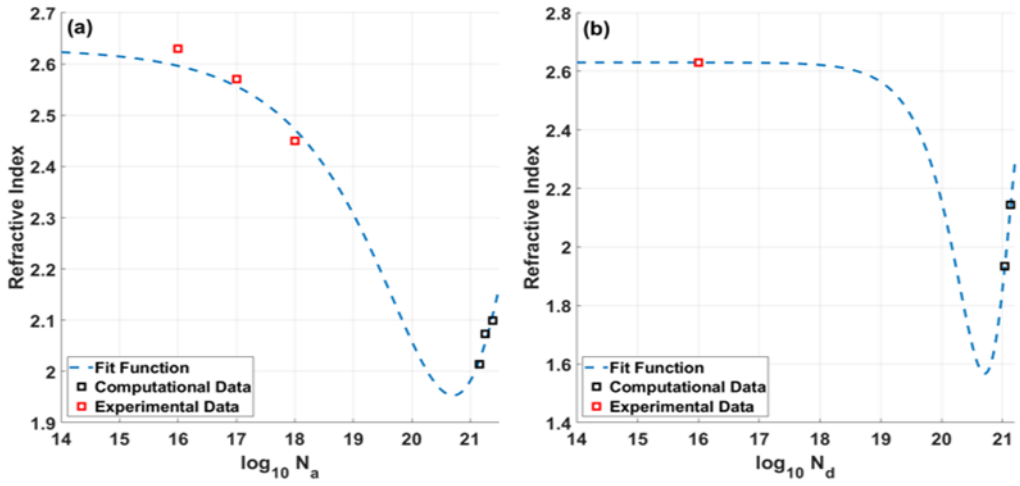

Figure A1 Refractive index (*n*) distribution of (a) Mg doped and (b) Si doped GaN with respect to acceptor and donor concentrations (N_a/N_d, cm^{-3}), respectively

Table A1 Refractive index (c) and critical concentration value (μ) of GaN, fit-function parameters of refractive index distributions, refractive index and extinction coefficient values for Mg and Si doped GaN are given for $\lambda = 367$ nm and $N = 2.00 \times 10^{20}$ cm^{-3}

Doped GaN	c (n_{GaN})	a_1	a_2	a_3	μ	**Refractive Index (*n*)**	**Extinction Coefficient (k)**
Mg:GaN	2.63	1.7395	1.1087	2.2097	20.3	1.994	0.190
Si:GaN	2.63	7.8616	2.6735	3.7836	20.3	1.862	0.112

Acknowledgments
The nanostructure quantum electronic simulation *nextnano* has been employed in the first optimization step on internal quantum efficiency. We would like to thank Dr. Stefan BIRNER and the team for their understanding and contribution in using the package.

Funding
The authors have no received any financial support for the research, authorship or publication of this study.

The Declaration of Conflict of Interest/ Common Interest
No conflict of interest or common interest has been declared by the authors.

Authors' Contribution
The first author contributed 30% to this study and remaining 70% has been shared as 25% by both the second and third authors, and 20% by the fourth author.

The Declaration of Ethics Committee Approval
This study does not require ethics committee permission or any special permission.

The Declaration of Research and Publication Ethics
The authors of the paper declare that they comply with the scientific, ethical and quotation rules of SAUJS in all processes of the paper and that they do not make any falsification on the data collected. In addition, they declare that Sakarya University Journal of Science and its editorial board have no responsibility for any ethical violations that may be encountered, and that this study has not been evaluated in any academic publication environment other than Sakarya University Journal of Science.

REFERENCES

[1] X. Han, Y. Zhang, P. Li, L. Yan, G. Deng, L. Chen, Y. Yu, J. Yin, "Fabrication of vertically conducting near ultraviolet LEDs on SiC substrates," Superlattices and Microstructures, vol. 125, pp. 348-355, 2018.

[2] T. Wu, Q. Zha, W. Chen, Z. Xu, T. Wang, X. He, "Development and deployment of a cavity enhanced UV-LED spectrometer for measurements of atmospheric HONO and NO2 in Hong Kong," Atmospheric Environment, vol. 95, pp. 544-55, 2014.

[3] A. M. Suhail, M. J. Khalifa, N. M. Saeed, O. A. Ibrahim, "White light generation from CdS nanoparticles illuminated by UV-LED," The European Physical Journal Applied Physics, vol. 49, p. 30601, 2010.

[4] O. Rodenko, H. Fodgaard, P. T. Lichtenberg, M. Petersen, C. Pedersen, "340 nm pulsed UV LED system for europium-based time-resolved fluorescence detection of immunoassays," Optics Express, vol. 24, no. 19, pp. 22135-22143, 2016.

[5] Y. Thana, A. Ngamjarurojana, D. Boonyawan, "Analysis of cold atmospheric-pressure bio-medicine plasmas by using UV absorption spectroscopy," Surface & Coatings Technology, vol. 306, pp. 106-112, 2016.

[6] J. Xu, C. Wu, Z. Yang, W. Liu, H. Chen, K. Batool, J. Yao, X. Fan, J. Wu, W. Rao, T. Huang, L. Xu, X. Guan, L. Zhang, "For: Pesticide biochemistry and physiology recG is involved with the resistance of Bt to UV," Pesticide Biochemistry and Physiology, vol. 167, p. 104599, 2020.

[7] P. O. Nyangaresi, Y. Qina, G. Chen, B. Zhang, Y. Lu, L. Shen, "Comparison of UV-LED photolytic and UV-LED/TiO_2 photocatalytic disinfection for Escherichia coli in water," Catalysis Today, vol. 335, pp. 200-207, 2019.

[8] Y. Muramoto, M. Kimura, S. Nouda, "Development and future of ultraviolet light-emitting diodes: UV-LED will replace the UV lamp," Semiconductor Science and Technology, vol. 29, no. 8, p. 084004, 2014.

[9] M. A. S. Ibrahim, J. MacAdam, O. Autin, B. Jefferson, "Evaluating the Impact of LED Bulb Development on the Economic Viability of Ultraviolet Technology for Disinfection," Environmental Technology, vol. 35, pp. 400–406, 2014.

[10] A. Khan, K. Balakrishnan, T. Katona, "Ultraviolet light-emitting diodes based on group three nitrides," Nature Photonics, vol. 2, pp. 77-84, 2008.

[11] M. Kneissl, T. Kolbe, C. Chua, V. Kueller, N. Lobo, J. Stellmach, A. Knauer, H. Rodriguez, S. Einfeldt, Z. Yang, N. M. Johnson, M. Weyers, "Advances in group III-nitride-based deep UV light-emitting diode technology," Semiconductor Science and Technology, vol. 26, pp. 014036, 2011.

[12] L. Dimitrocenko, J. Grube, P. Kulis, G. Marcins, B. Polyakov, A. Sarakovskis, M. Springis, I. Tale, "AlGaN–InGaN–GaN Near Ultraviolet Light Emitting Diode," Latvian Journal of Physics and Technical Sciences, vol. 45, no. 4, 2008.

[13] Y. Li, Z. Xing, Y. Zheng, X. Tang, W. Xie, X. Chen, W. Wang, G. Li, "High-efficiency near-UV light-emitting diodes on Si substrates with InGaN/GaN/AlGaN/GaN multiple quantum wells" Journal of Materials

Chemistry C, vol. 8, no. 3, pp. 883-888, 2020.

[14] L. R. Chen, S. C. Huang, J. L. Chiu, C. C. Lu, W. M. Su, C. Y. Weng, H. Y. Shen, T. C. Lu, H. Chen, "Degradation mechanisms of bias stress on nitride-based near-ultraviolet light-emitting diodes in salt water vapor ambient," Microelectronic Engineering, vol. 218, no. 111158, 2019.

[15] M. A. Khan, "AlGaN multiple quantum well based deep UV LEDs and their applications," Physica Status Solidi A, vol. 203, no. 7, pp. 1764-1770, 2006.

[16] A. Sandhu, "The future of ultraviolet LEDs," Nature Photonics, vol. 1, no. 1, p. 38, 2007.

[17] P. Li, H. Li, L. Wang, X. Yi, G. Wang, "High Quantum Efficiency and Low Droop of 400-nm InGaN Near-Ultraviolet Light-Emitting Diodes Through Suppressed Leakage Current," IEEE Journal of Quantum Electronics, vol. 51, no. 9, p. 3300605, 2015.

[18] A. B. M. H. Islam, D. S. Shim, J. I. Shim, "Enhanced Radiative Recombination Rate by Local Potential Fluctuation in InGaN/AlGaN Near-Ultraviolet Light-Emitting Diodes," Applied Sciences, vol. 9, no. 5, p. 871, 2019.

[19] H. Hu, S. Zhou, X. Liu, G. Yilin, C. Gui, S. Liu, "Effects of GaN/AlGaN/Sputtered AlN nucleation layers on performance of GaN-based ultraviolet light-emitting diodes," Scientific Reports, vol. 7, p. 44627, 2017.

[20] X. H. Yong, C. X. Fang, P. Yan, X. M. Sheng, S. Yan, H. X. Bo, X. X. Gang, "Progress in research of GaN-based LEDs fabricated on SiC substrate," Chinese Physics B, vol. 24, no. 6, p. 067305, 2015.

[21] M. Lee, M. Yang, K. M. Song, S. Park, "InGaN/GaN Blue Light Emitting Diodes Using Freestanding GaN Extracted from a Si Substrate," American Chemical Society Photonics, vol. 5, no. 4, pp. 1453–1459, 2018.

[22] V. K. Malyutenko O. Y. Malyutenko, "Do we need to recalibrate our strategy in InGaN-on-SiC LED technology given its low efficiency," Proceedings of the Society of Photo-Optical Instrumentation Engineers (SPIE), vol. 9768, p. 97681N, 2016.

[23] M. Kim, T. Fujita, S. Fukahori, T. Inazu, C. Pernot, Y. Nagasawa, A. Hirano, M. Ippommatsu, M. Iwaya, T. Takeuchi, S. Kamiyama, M. Yamaguchi, Y. Honda, H. Amano, I. Akasaki, "AlGaN-Based Deep Ultraviolet Light-Emitting Diodes Fabricated on Patterned Sapphire Substrates," Applied Physics Express, vol. 4, no. 9, p. 092102, 2011.

[24] T. Takayoshi, M. Takuya, S. Jun, N. Norimichi, T. Kenji, H. Hideki, "Deep-ultraviolet light-emitting diodes with external quantum efficiency higher than 20% at 275 nm achieved by improving light-extraction efficiency," Applied Physics Express, vol. 10, no. 3, p. 031002, 2017.

[25] W. Lee, M. H. Kim, D. Zhu, A. N. Noemaun, J. K. Kim, E. F. Schubert, "Growth and characteristics of GaInN/GaInN multiple quantum well light-emitting diodes," Journal of Applied Physics, vol. 107, p. 063102, 2010.

[26] W. Y. Ching, Y. N. Xu, P. Rulis, L. Ouyang, "The electronic structure and spectroscopic properties of 3C, 2H, 4H, 6H, 15R and 21R polymorphs of SiC," Materials Science and Engineering: A, vol. 422, no. 1-2, pp. 147-156, 2006.

[27] P. Tao, H. Liang, X. Xia, Y. Liu, J. Jiang, H. Huang, Q. Feng, R. Shen, Y. Luo, G. Du, "Enhanced output power of near-ultraviolet LEDs with Al-GaN/GaN distributed Bragg reflectors on 6H–SiC by metal-organic chemical vapor deposition" Superlattices and Microstructures, vol.85, pp. 482-487, 2015.

[28] C. Yao, X. Ye, R. Sun, G. Yang, J. Wang, Y. Lu, P. Yan, J. Cao, S. Gao, "High-performance AlGaN-based solar-blind avalanche photodiodes with dual-periodic III–nitride distributed Bragg reflectors," Applied Physics Express, vol. 10, no. 3, p. 034302, 2017.

[29] X. Lu, J. Li, K. Su, C. Ge, Z. Li, T. Zhan, G. Wang, J. Li, "Performance-Enhanced 365 nm UV LEDs with Electrochemically Etched Nanoporous AlGaN Distributed Bragg Reflectors," Nanomaterials, vol. 9, no. 6, p. 862, 2019.

[30] A. Trellakis, T. Zibold, T. Andlauer, S. Birner, R. K. Smith, R. Morschl, P. Vogl, "The 3D nanometer device project nextnano: Concepts, methods, results" Journal of Computational Electronics, vol. 5, pp. 285–289, 2006.

[31] S. Birner, T. Zibold, T. Andlauer, T. Kubis, M. Sabathil, A. Trellakis, P. Vogl, "Nextnano: General Purpose 3-D Simulations," IEEE Transactions on Electron Devices, vol. 54, no. 9, pp. 2137-2142, 2007.

[32] M. D. Segall, P. J. D. Lindan, M. J. Probert, C. J. Pickard, P. J. Hasnip, S. J. Clark, M. C. Payne, "First-principles simulation: ideas, illustrations and the CASTEP code," Journal of Physics: Condensed Matter, vol. 14, no. 11, p. 2717, 2002.

[33] S. G. Johnson, J. D. Joannopoulos, "Block-iterative frequency-domain methods for Maxwell's equations in a planewave basis," Optics Express, vol. 8, no. 3, pp. 173-190, 2001.

[34] A. F. Oskooi, D. Roundy, M. Ibanescu, P. Bermel, J. D. Joannopoulos, S. G. Johnson, "Meep: A flexible free-software package for electromagnetic simulations by the FDTD method," Computer Physics Communications, vol. 181, no. 3, pp. 687-702, 2010.

[35] Y. R. Wu, C. Y. Huang, Y. Zhao, J. Speck, "Nonpolar and semipolar LEDs," in Nitride Semiconductor Light-Emitting Diodes (LEDs) -Materials, Technologies, and Applications-Woodhead Publishing Series in Electronic and Optical Materials, J. Huang, H.-C. Kuo, and S.-C. Shen, Eds. second ed., Cambridge, United Kingdom: Woodhead Pub., 2018, pp. 273-295.

[36] Z. H. Zhang, Y. Zhang, W. Bi, H. V. Demir, X. W. Sun, "On the internal quantum efficiency for InGaN/GaN light-emitting diodes grown on insulating substrates," Physica Status Solidi A, vol. 213, no. 12, pp. 3078-3102, 2016.

[37] C. Haller, J. F. Carlin, G. Jacopin, D. Martin, R. Butte, N. Grandjean, "Burying non-radiative defects in InGaN underlayer to increase InGaN/GaN quantum well efficiency," Applied Physics Letters, vol. 111, p. 262101, 2017.

[38] S. Pearton, GaN and ZnO-based Materials and Devices. Gainesville, USA: Springer, 2012.

[39] S. Chiaria, E. Furno, M. Goano, E. Bellotti, "Design Criteria for Near-Ultraviolet GaN-Based Light-Emitting

Diodes," IEEE Transactions on Electron Devices, vol. 57, no. 1, pp. 60-70, 2010.

[40] R. Ramesh, P. Arivazhagan, M. Jayasakthi, R. Loganthan, K. Prabakaran, B. Kuppuligam, M. Balaji, K. Baskar, "Structural optical and electrical studies of AlGaN/GaN heterostructures with AlN interlayer grown on sapphire substrate by MOCVD," in Physics of Semiconductor Devices, V. K. Jain and A. Verma, Eds. first ed., New York, USA: Springer, 2013, pp. 119-120.

[41] M. E. Zvanut, Y. Uprety, J. Dashdorj, M. Moseley, W. A. Doolittle, "Passivation and activation of Mg acceptors in heavily doped GaN" Journal of Applied Physics, vol. 110, no. 4, p. 044508, 2001.

[42] H. Hu, S. Zhou, X. Liu, Y. Gao, C. Gui, S. Liu, "Effects of GaN/AlGaN/Sputtered AlN nucleation layers on performance of GaN-based ultraviolet light-emitting diodes," Scientific Reports, vol.7, p. 44627, 2017.

[43] S. Z. Aftab, N. Khalid, "A novel approach to enhance performance efficiency of AlGaN/InGaN based MQW LED in UV-region," 2019 16th International Bhurban Conference on Applied Sciences and Technology (IBCAST), 2019, pp. 20-25.

[44] X. A. Cao, S. F. LeBoeuf, M. P. D'Evelyn, S. D. Arthur, J. Kretchmer, "Blue and near-ultraviolet light-emitting diodes on free-standing GaN substrates," Applied Physics Letters, vol. 84, p. 4313, 2004.

[45] H. Hirayama, K. Akita, T. Kyono, T. Nakamura, K. Ishibashi, "High-efficiency 352 nm quaternary InAlGaN-based ultraviolet light-emitting diodes grown on GaN substrates" The Japan Society of Applied Physics, vol. 43, no. 10, p. L1241, 2004.

[46] J. P. Perdew, A. Ruzsinszky, G. I. Csonka, O. A. Vydrov, G. E. Scuseria, L. A. Constantin, X. Zhou, K. Burke, "Restoring the density-gradient expansion for exchange in solids and surfaces," Physical Review Letters, vol. 100, no. 136406, 2008.

[47] L. S. Pedroza, J. R. Silva, K. Capelle, "Gradient-dependent density functionals of the Perdew-Burke-Ernzerhof type for atoms, molecules, and solids," Physical Review B, vol. 79, no. 201106, 2009.

[48] P. Haas, F. Tran, P. Blaha, "Calculation of the lattice constant of solids with semilocal functionals," Physical Review B, vol. 79, no. 085104, 2009.

[49] L. Schimka, J. Harl, G. Kresse, "Improved hybrid functional for solids: The HSEsol functional," Journal of Chemical Physics, vol. 134, p. 024116, 2011.

[50] H. J. Monkhorst, J. D. Pack, "Special points for Brillouin-zone integrations" Physical Review B, vol. 13, p. 5188, 1976.

[51] A. Bauer, P. Reischauer, J. Krausslich, N. Schell, W. Matz, K. Goetz, "Structure refinement of the silicon carbide polytypes 4H and 6H: unambiguous determination of the refinement parameters," Acta Crystallographica Section A, vol. 57, pp. 60-67, 2001.

[52] G. C. Capitani, S. D. Pierro, G. Tempesta, "The 6H-SiC structure model: Further refinement from SCXRD data from a terrestrial moissanite," American Mineralogist, vol. 92, no. 2-3, pp. 403–407, 2007.

[53] A. D. Alvarenga, M. Grimsditch, "Raman scattering from cubic boron nitride up to 1600 K," Journal of Applied Physics, vol. 72, p. 1955, 1992.

[54] H. Schulz, K. H. Thiemann, "Crystal structure refinement of AlN and GaN," Solid State Communications, vol. 23, no. 11, pp. 815-819, 1977.

[55] M. E. Levinshtein, S. L. Rumyantsev, M. S. Shur, Properties of Advanced Semiconductor Materials: GaN, AIN, InN, BN, SiC, SiGe. New York, USA: John Wiley & Sons, Inc., 2001.

[56] J. Li, K. B. Nam, M. L. Nakarmi, J. Y. Lin, H. X. Jiang, "Band structure and fundamental optical transitions in wurtzite AlN," Applied Physics Letters, vol. 83, p. 5163, 2003.

[57] S. Strite H. Morkoç, "GaN, AlN, and InN: A review," Journal of Vacuum Science & Technology B Microelectronics and Nanometer Structures Processing, Measurement, and Phenomena, vol. 10, p. 1237, 1992.

[58] M. Feneberg, S. Osterburg, M. F. Romero, B. Garke, R. Goldhahn, M. D. Neumann, J. Yan, J. Zeng, J. Wang, J. Li, "Optical properties of magnesium doped AlxGa1− xN (0.61≤x≤ 0.73)," Journal of Applied Physics, vol. 116, no. 14, p. 143103, 2014.

[59] C. Buchheim, R. Goldhahn, M. Rakel, C. Cobet, N. Esser, U. Rossow, D. Fuhrmann, A. Hangleiter, "Dielectric function and critical points of the band structure for AlGaN alloys," Physica Status Solidi (b), vol. 242, no. 13, pp. 2610-2616, 2005.

[60] J. F. Muth, J. D. Brown, M. A. L. Johnson, Z. Yu, R. M. Kolbas, J. W. Cook, J. F. Schetzina, "Absorption coefficient and refractive index of GaN, AlN and AlGaN alloys," Materials Research Society Internet Journal of Nitride Semiconductor Research, vol. 4, no. S1, pp. 502-507, 1999.

[61] P. Prajoon, D. Nirmal, M. A. Menokey, J. C. Pravin, "Efficiency Enhancement of InGaN MQW LED Using Compositionally Step Graded InGaN Barrier on SiC Substrate," Journal of Display Technology, vol. 12, no. 10, p. 1237, 2016.

[62] J. P. Perdew, K. Burke, M. Ernzerhof, "Generalized Gradient Approximation Made Simple," Physical Review Letters, vol. 77, no. 3865, p. 1396, 1996.

[63] S. J. Clark, M. D. Segall, C. J. Pickard, P. J. Hasnip, M. I. J. Probert, K. Refson, M. C. Payne, "First principles methods using CASTEP," Zeitschrift für Kristallographie - Crystalline Materials, vol. 220, no. 5-6, pp. 567-570, 2009.

[64] C. Chen, K. C. Cheng, E. Chagarov, J. Kanicki, "Crystalline In–Ga–Zn–O Density of States and Energy Band Structure Calculation Using Density Function Theory," Japanese Journal of Applied Physics, vol. 50, no. 9, p. 091102, 2011.

[65] J. M. M. Duart, R. J. M. Palma, F. A. Rueda, Nanotechnology for Microelectronics and Optoelectronic. Amsterdam, The Netherlands: Elsevier, 2006.

[66] D. Vanderbilt, "Soft self-consistent pseudopotentials in a generalized eigenvalue formalism," Physical Review B, vol. 41, p. 7892, 1990.

[67] J. M. Hu, S. P. Huang, Z. Xie, H. Hu, W. D. Cheng, "First-principles study of the elastic and optical properties of the pseudocubic Si_3As_4, Ge_3As_4 and

Sn_3As_4," Journal of Physics: Condensed Matter, vol. 19, no. 49, p. 496215, 2007.

[68] R. Ruppin, "Evaluation of extended Maxwell-Garnett theories," Optics Communications, vol. 182, no. 4-6, pp. 273-279, 2000.

[69] G. Liu, J. Zhang, C. K. Tan, N. Tansu, "Efficiency-Droop Suppression by Using Large-Bandgap AlGaInN Thin Barrier Layers in InGaN Quantum-Well Light-Emitting Diodes," IEEE Photonics Journal, vol. 5, no. 2, p. 2201011, 2013.

[70] S. Xu, C. Xu, Y. Liu, Y. Hu, R. Yang, Q. Yang, J. H. Ryou, H. J. Kim, Z. Lochner, S. Choi, R. Dupuis, Z. L. Wang, "Ordered Nanowire Array Blue/Near-UV Light Emitting Diodes," Advanced Materials, vol. 22, no. 42, pp. 4749-4753, 2010.

[71] W. K. Bae, Y. S. Park, J. Lim, D. Lee, L. A. Padilha, H. McDaniel, I. Robel, C. Lee, J. M. Pietryga, V. I. Klimov, "Controlling the influence of Auger recombination on the performance of quantum-dot light-emitting diodes," Nature Communications, vol. 4, p. 2661, 2013.

[72] C. Jia, T. Yu, X. Feng, K. Wang, G. Zhang, "Performance improvement of GaN-based near-UV LEDs with InGaN/AlGaN superlattices strain relief layer and AlGaN barrier," Superlattices and Microstructures, vol. 97, pp. 417-423, 2016.

[73] H. Morkoç, Ü. Özgür, "Zinc Oxide: Fundamentals, Materials and Device Technology," Weinheim, Germany: John Wiley & Sons, 2008.

[74] V. Laino, F. Roemer, B. Witzigmann, C. Lauterbach, Ulrich T. Schwarz, C. Rumbolz, M. O. Schillgalies, M. Furitsch, A. Lell, V. Harle, "Substrate modes of (Al, In) GaN semiconductor laser diodes on SiC and GaN substrates," IEEE Journal of Quantum Electronics, vol. 43, no. 1, pp. 16-24, 2007.

[75] G. A. Smolyakov, P. G. Eliseev, M. Osinski, "Effects of resonant mode coupling on optical Characteristics of InGaN-GaN-AlGaN lasers," IEEE Journal of Quantum Electronics, vol. 41, no. 4, pp. 517-524, 2005.

[76] H. Y. Peng, M. D. McCluskey, Y. M. Gupta, M. Kneissl, N. M. Johnson, "The Franz–Keldysh effect in shocked GaN: Mg," Applied Physics Letters, vol. 82, no. 13, pp. 2085-2087, 2003.

[77] S. R. Bhattacharyya, A. K. Pal, "Electrical and optical properties of silicon-doped gallium nitride polycrystalline films," Bulletin of Materials Science, vol. 31, no. 1, pp. 73-82, 2008.

[78] J. Piprek, H. Wenzel, M. Kneissl, "Analysis of wavelength-dependent performance variations of GaN-based ultraviolet lasers," International Society for Optics and Photonics In Optoelectronic Devices: Physics, Fabrication, and Application IV, vol. 6766, p. 67660, 2007.

[79] O. Ambacher, W. Rieger, P. Ansmann, H. Angerer, T. D. Moustakas, M. Stutzmann, "Sub-bandgap absorption of gallium nitride determined by photothermal deflection spectroscopy," Solid State Communications, vol. 97, no. 5, pp. 365-370, 1996.

[80] A. Cremades, L. Görgens, O. Ambacher, M. Stutzmann, F. Scholz, "Structural and optical properties of Si-doped GaN," Physical Review B, vol. 61, no. 4, p. 2812, 2000.